Sensors and Materials, Vol. 34, No. 9 (2022) 3491–3502
MYU Tokyo

S & M 3055

Impact of Improved Wire Tension Stability on Wire Electrical Discharge Machining Precision

Pi-Wen Wang* and Chao-Lun Liu

Huafan University, No. 1 Huafan Rd., Shihding Dist., New Taipei City 223011, Taiwan (R.O.C.)

(Received March 29, 2022; accepted June 13, 2022)

Keywords: WEDM, wire transport system, wire tension, straightness

We propose a system dynamic approach for improving the stability of wire electrical discharge machining (WEDM). The approach includes wire spool inertia isolation and a damped sandwich mechanism, which increase the fundamental frequency and damping coefficient of the system, respectively. Thus, the wire tension stability is also improved. We establish a dynamic model to simulate the dynamic behavior of the wire transport system. Then the wire tension stability is optimized through tuning the damping material parameters of the damped sandwich mechanism. The mechanism was mounted on a commercial WEDM machine to show the benefits in terms of wire tension and machining precision. Results show that the maximum overshoot of wire tension was reduced by 51% and the steady-state wire tension variation was improved from 176 to 48 gf. When cutting 10-cm-thick SKD11 tool steel, the deviation from a straight line was reduced by 45%.

1. Introduction

Wire electrical discharge machining (WEDM) plays an important role in numerous ultra-precision industries. During the process, the wire behavior is affected by several interactions,[1] including a series of discrete explosive forces induced by the collapse of gas bubbles,[2] electrostatic force, electromagnetic forces, and flushing pressure. Under these forces, the wire suffers flexing and vibration,[3] resulting in errors in the machined part, such as a corner error,[4] drum shape,[5,6] non-uniform kerf, and poor surface finish. Accuracy can be greatly improved through multiple trim cuts. However, trim cuts are inefficient as the deviation of the first cut is significant. To eliminate the inaccuracy, many investigations have focused on tuning factors in WEDM, including dielectric pressure, wire tension, pulse parameters, wire feed rate, and cutting rate.[7–9] For example, the corner error is reduced by reducing the cutting speed, pulse energy, and flushing pressure toward the corner. Meanwhile, the wire tension is raised to as high as possible to enhance the wire rigidity. Once a corner is rounded, these parameters are restored to their original values. Using a set of optimal parameters can reduce the corner error by 50%.[9]

Among numerous machining factors, stable wire tension has been demonstrated to be more effective than the other factors in reducing wire flexing and geometry errors.[10–13] Machine manufacturers currently use servo tension control systems[14–16] to solve this problem. The

*Corresponding author: e-mail: meewpw@cc.hfu.edu.tw
https://doi.org/10.18494/SAM3926

ISSN 0914-4935

system comprises two servo motors, one mounted on the wire supply reel and the other mounted on the windup reel. A swing arm sensor is employed to stabilize the wire tension by tuning the feed rate and windup rate. According to Fanuc's twin servo wire tension control,[16] the variation of the tension can be reduced to less than one-quarter of that of an open-loop system.[17,18] In addition, the slow reaction of the servo motor is capable of reducing the variation of the tension at low frequencies. However, high-frequency variation cannot be reduced, thus reducing performance.

We previously developed two methods to improve wire tension stability.[11,12] The first method was to employ an angle sensor to keep the wire feed rate in sync with the windup rate. The wire spool inertia was isolated from the wire transport system, thus greatly increasing the fundamental frequency of the system. The second method was to develop a damped sandwich mechanism (DSM) to increase the damping factor of the wire transport system. After mounting wire spool isolation and DSM on the system, the wire tension variation was reduced by 80%. Compared with servo wire tension control systems, both devices are cost-effective and easily mounted on a commercial WEDM machine. However, the damping material parameters of the DSM, including the stiffness and damping coefficient, were not investigated. As reported in this paper, a dynamic model of the wire transport system is constructed and the effect of the DSM parameters on the system behavior is studied. Finally, the performances of the DSM are validated through cutting a workpiece of 10 cm thickness.

2. Theory

The wire transport system of a WEDM machine is illustrated in Fig. 1. As the windup reel operates, the wire moves from the wire spool and passes through stages a to i to the waste bin.

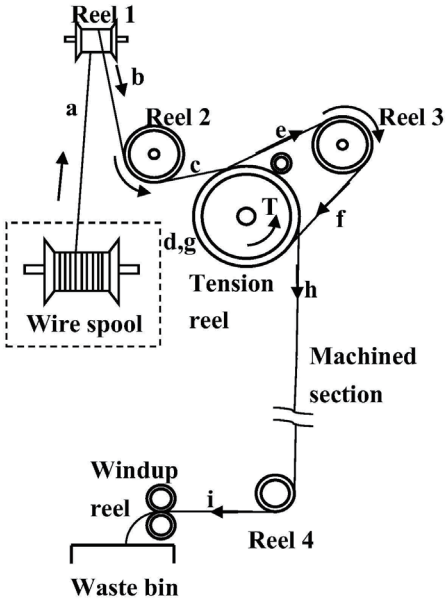

Fig. 1. Wire transport system of WEDM.

Reel 1 is used to ensure a smooth connection between the wire spool and reel 2. Reels 2 and 3 are V-groove reels placed on both sides of the tension reel. The V-grooves are used to prevent the wire from jumping the rim of the tension reel. The tension reel is connected to a magnetic powder brake, which generates the wire tension through voltage-induced friction.

2.1 Isolation of wire spool inertia

In the wire transport system, all idle reels are passively rotated by the friction from the moving wire. Hence, each reel inertia can be regarded as an individual inertial element in the system. In the wire transport system, the wire spool inertia is ten times greater than that of the other reels and induces an extremely low resonance frequency. Hence the system is easily disturbed by tiny perturbations.

To solve this problem, we previously proposed the concept of wire spool inertia isolation as shown in Fig. 2. The apparatus used includes an angle sensor, a pulse-width modulation generator, and a wire feed motor M_1. As the windup motor M_3 operates, the wire between the wire spool and tension reel M_2 is gradually tensed, forcing the angle θ to increase. The angle sensor outputs an increasing voltage to increase the speed of motor M_1. In this way, the wire feed rate is kept in sync with the windup rate so that the wire between the wire spool and tension reel remains relaxed. The wire spool inertia can be isolated from the wire transport system so that the fundamental frequency of the system can be greatly increased.

2.2 Damped sandwich mechanism

A DSM is proposed to increase the damping factor of the system as shown in Fig. 3. The mechanism is composed of a base, two fixed reels, and a moving reel whose axis is connected to a damped sandwich beam. The damped sandwich beam is composed of multiple viscoelastic layers sandwiched between elastic layers. Its spring constant and damping coefficient can be

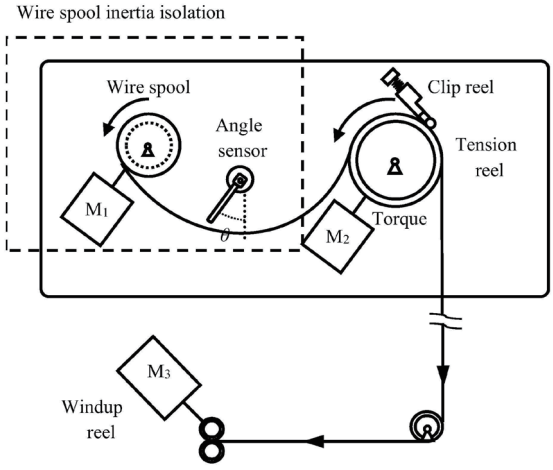

Fig. 2. Wire spool inertia isolation.

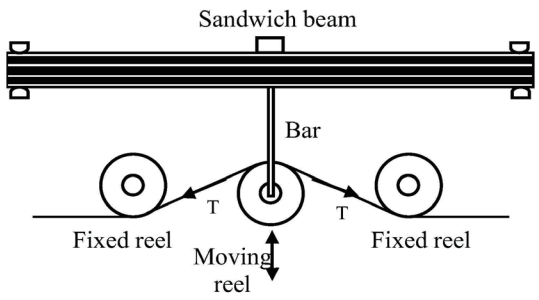

Fig. 3. Illustration of DSM.

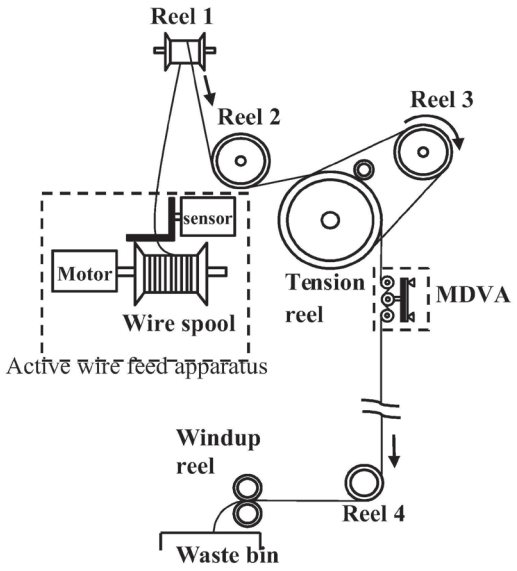

Fig. 4. Wire transport system with DSM.

tuned by adjusting the number of layers, shape geometries, materials, and so forth. The DSM is placed in front of the upper nozzle. The wire tension fluctuation is effectively attenuated through the oscillation of the sandwich beam. Mounting both devices on the wire transport system as shown in Fig. 4 increases the system stability due to the increased fundamental frequency and damping factor.

3. Physical Model of Wire Transport System

To study the performance of the DSM in the wire transport system, a physical model is built. The wire and reel in the system are respectively simulated as a spring element and a rotary inertia. The DSM is simplified to a spring-mass-damper system. The system is modeled as a multi-degree-of freedom (MDOF) system.

The rotary inertia of each reel and the spring constant of each wire segment can be expressed as

$$I_n = \frac{m_n r_n^2}{2}, \tag{1}$$

$$k_n = \frac{A_n E_n}{l_n}, \tag{2}$$

where I_n, m_n, and r_n represent the rotary inertia, mass, and radius of the nth reel, while A_n, E_n, and l_n are the cross section, Young's modulus, and length of each wire segment, respectively. Subscripts T and W respectively denote the tension reel and wire reel.

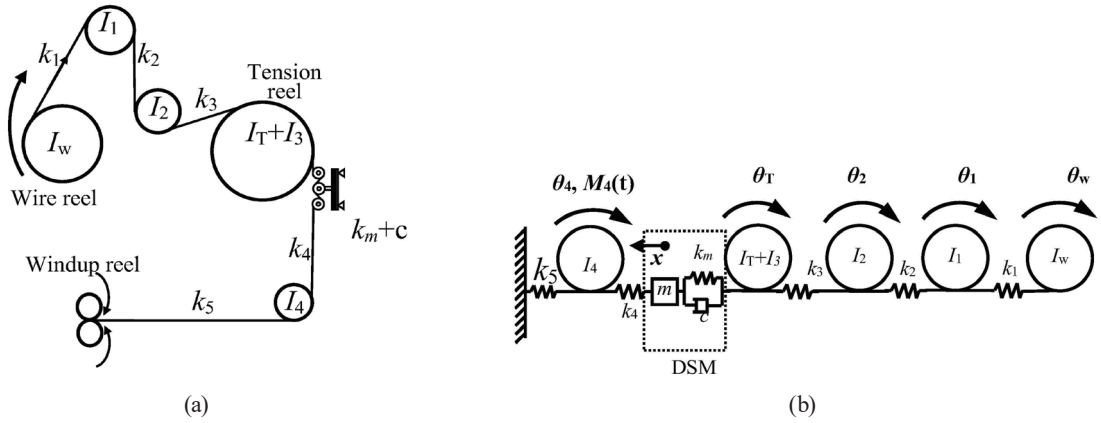

Fig. 5. (a) Illustration of wire transport system and (b) corresponding MDOF model.

The wire transport system can be simplified to that in Fig. 5(a) and modeled as a six-degree-of-freedom system as shown in Fig. 5(b), where *km*, *m*, and *c* are respectively the spring constant, mass, and damping coefficient of the DSM. If the wire spool inertia is isolated, the wire between the wire spool and the tension reel is relaxed. Hence, the rotary inertias of the wire spool, reel 1, and reel 2 can be ignored. The wire transport system can be modeled by specifying these reel inertias as infinitesimals.

The governing equation of the model illustrated in Fig. 5(b) is derived as follows. The equation of motion for reel 4 is

$$I_4\ddot{\theta}_4 = -r_4{}^2k_5\theta_4 - k_4r_4(r_4\theta_4 - x) + M_4, \tag{3}$$

where the first term on the right-hand side is the moment on I_4 due to k_5, while the second term is the moment due to k_4, and x is the deflection of the DSM. The third term is the external moment M_4. The equations of motion of the other reels are as follows.

$$(I_T + I_3)\ddot{\theta}_T = k_m r_T x - (k_m + k_3)r_T^2\theta_T + k_3r_2r_T\theta_2 + cr_T\dot{x} - r_T^2\dot{\theta}_T \tag{4}$$

$$I_2\ddot{\theta}_2 = k_3r_2r_T\theta_T - r_2^2(k_2 + k_3)\theta_2 + k_2r_1r_2\theta_1 \tag{5}$$

$$I_1\ddot{\theta}_1 = k_2r_1r_2\theta_2 - r_1^2(k_1 + k_2)\theta_1 + k_1r_1r_W\theta_W \tag{6}$$

$$I_W\ddot{\theta}_W = k_1r_Wr_1\theta_1 - r_w^2k_1\theta_W \tag{7}$$

In addition to the rotation of all reels, the DSM is a translation system whose equation of motion is

$$m\ddot{x} = k_4(r_4\theta_4 - x) - k_m(x - r_T\theta_T) - c(\dot{x} - r_T\dot{\theta}_T), \tag{8}$$

where m is the mass of reel 3, and k_m and c are respectively the spring constant and damping coefficient of the DSM. The first term on the right-hand side is the restoring force due to k_4, while the second and third terms are the restoring and damping forces due to the DSM, respectively. The model shown in Fig. 5(b) can be expressed in matrix form:

$$\boldsymbol{I}\ddot{\theta} + \boldsymbol{C}\dot{\theta} + \boldsymbol{K}\theta = \boldsymbol{M}, \tag{9}$$

where $\boldsymbol{\theta} = \{\theta_4, x, \theta_T, \theta_2, \theta_1, \theta_w\}^T$ is the angle of each reel and x is the displacement of the DSM; $\boldsymbol{M} = \{M_4(t), 0, 0, 0, 0, 0\}^T$ is the excitation and only reel 4 is assumed to be excited; $\boldsymbol{I}$ and $\boldsymbol{K}$ are the inertial and stiffness matrices, respectively, which can be expressed as

$$\boldsymbol{I} = \begin{bmatrix} I_4 & 0 & 0 & 0 & 0 & 0 \\ 0 & m & 0 & 0 & 0 & 0 \\ 0 & 0 & I_T & 0 & 0 & 0 \\ 0 & 0 & 0 & I_2 & 0 & 0 \\ 0 & 0 & 0 & 0 & I_1 & 0 \\ 0 & 0 & 0 & 0 & 0 & I_w \end{bmatrix}, \tag{10}$$

$$\boldsymbol{K} = \begin{bmatrix} (k_4 + k_5)r_4^2 & -k_4 r_4 & 0 & 0 & 0 & 0 \\ -k_4 r_4 & k_4 + k_m & -k_m r_T & 0 & 0 & 0 \\ 0 & -k_m r_T & (k_3 + k_m)r_T^2 & -k_3 r_2 r_T & 0 & 0 \\ 0 & 0 & -k_3 r_2 r_T & (k_2 + k_3)r_2^2 & -k_2 r_1 r_2 & 0 \\ 0 & 0 & 0 & -k_2 r_1 r_2 & (k_1 + k_2)r_1^2 & -k_1 r_1 r_W \\ 0 & 0 & 0 & 0 & -k_1 r_1 r_W & k_1 r_W^2 \end{bmatrix}. \tag{11}$$

$\boldsymbol{C}$ is the damping matrix resulting from the damping coefficient of the DSM and is expressed as

$$\boldsymbol{C} = \begin{bmatrix} 0 & 0 & 0 & 0 & 0 & 0 \\ 0 & c & -cr_T & 0 & 0 & 0 \\ 0 & -cr_T & cr_T^2 & 0 & 0 & 0 \\ 0 & 0 & 0 & 0 & 0 & 0 \\ 0 & 0 & 0 & 0 & 0 & 0 \\ 0 & 0 & 0 & 0 & 0 & 0 \end{bmatrix}. \tag{12}$$

The frequency response of the wire transport system can be obtained by substituting the excitation and response as harmonic functions. Equation (9) can be expressed as

$$\left[\boldsymbol{K} - \omega^2 \boldsymbol{I} + i\omega \boldsymbol{C}\right]\theta = M, \tag{13}$$

where $\boldsymbol{\theta} = \{\theta_4, X, \theta_T, \theta_2, \theta_1, \theta_w\}^T$ is the amplitude of $\boldsymbol{\theta}$, $\boldsymbol{M} = \{1, 0, 0, 0, 0, 0\}^T$ is the amplitude of $\boldsymbol{M}$, and ω is the excitation frequency. Then the response can be obtained as

$$\theta = \left[\boldsymbol{K} - \omega^2 \boldsymbol{I} + i\omega \boldsymbol{C}\right]^{-1} \boldsymbol{M}. \tag{14}$$

After solving Eq. (13), the variation of the wire tension T in the machining section can be expressed as

$$T = k_4(r_4\theta_4 - x). \tag{15}$$

4. Numerical Simulation

4.1 Frequency response of wire tension

After deriving the governing equation, the dynamic behavior of the system is simulated. The rotational inertia of the wire spool is easily simulated by designating the wire spool, reel 1, and reel 2 inertias as infinitesimals. On the other hand, the effect of the DSM is removed by setting an extremely large value for its spring constant.

The parameters of the wire transport system are listed in Tables 1 and 2. The mass, spring constant, and damping ratio of the DSM are m = 20 g, k_m = 1600.0 N/m, and ξ = 0.2, respectively. The wire diameter and Young's modulus are 25 μm and 1.1 × 10^{11} N/m^2, respectively. A harmonic torque with 1 Nm amplitude is located at reel 4 and the frequency response of the wire tension is shown in Fig. 6. The results show that the fundamental frequency of the original system is 4.1 Hz. After isolating the wire spool inertia, the fundamental frequency rises to

Table 1
Parameters of the wire transport system (reels).

Parameter	Wire spool (I_W)	Idle reel 1 (I_1)	Idle reels 2,3 (I_2, I_3)	Tension reel (I_T)
Mass (kg)	5.0	0.35	0.04	1.0
Diameter (m)	0.12	0.09	0.085	0.14
Thickness (m)	0.2	0.15	0.015	0.025

Table 2
Parameters of the wire transport system (wires).

	Segment 1 (k_1)	Segment 2 (k_2)	Segment 3 (k_3)	Segment 4 (k_4)	Segment 5 (k_5)
Length (cm)	33	18	20	110	100

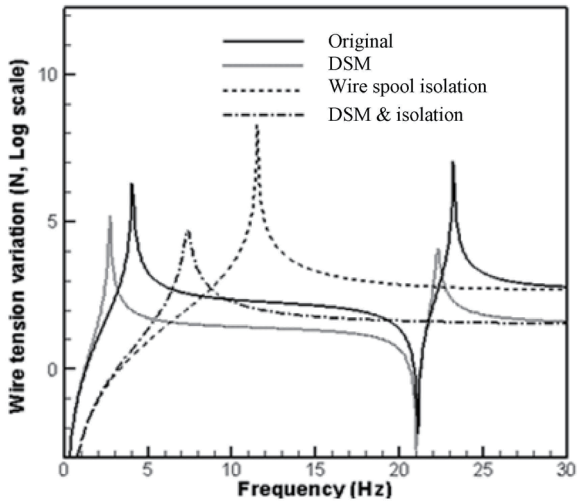

Fig. 6. Frequency responses of four wire transport systems.

11.5 Hz. The result shows that the wire spool inertia significantly decreases the fundamental frequency of the system. Using the DSM, the fundamental frequency decreases to 2.2 Hz. Although the magnitude of the resonant peak is also slightly reduced, the extremely low fundamental frequency reduces the stability of the wire tension.

Once the wire spool inertia is isolated and the DSM is mounted on the system, the fundamental frequency is 7.2 Hz and the resonance peak is also greatly reduced. The result shows that the DSM is a flexible mechanism that decreases system rigidity but can greatly increase system damping. However, a very low DSM stiffness may lead to system instability due to the low fundamental frequency. Thus, DSM stiffness is critical to system stability, and the next section presents a parametric study of DSM stiffness.

4.2 DSM behavior in wire transport system

From the previous section, the wire spool inertia plays a major role in reducing system resonance, and the DSM further enhances the damping coefficient of the system. However, improper DSM parameters may also decrease the fundamental frequency of the system, thus inducing instability. To optimize the performance of the DSM, its spring constant is used as the design parameter, and the mass m and damping ratio ξ are fixed as 20 g and 0.2, respectively. Through tuning the spring constant k_m, the damping coefficient is obtained as $2\xi\sqrt{k_m m}$. Then, the modal loss factor (first mode) and time constant of the wire transport system are obtained. Systems with and without the wire spool inertia under different DSM spring constants are investigated.

Figure 7 illustrates the modal loss factor, defined as the ratio of the frequency ω_n to the difference between the two frequencies ($\omega_2 - \omega_1$) on either side (3 dB below the peak amplitude) of the resonance. The maximal value occurs because of the very small spring constant. Although the damping coefficient of the DSM is relatively small, the displacement of the DSM is so large

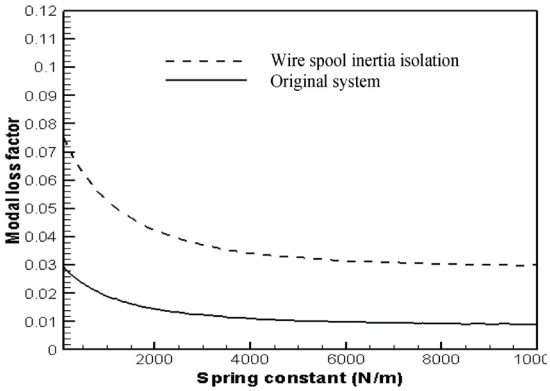

Fig. 7. Modal loss factor with respect to spring constant of DSM.

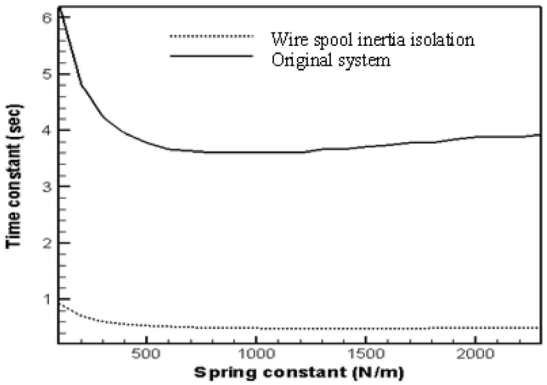

Fig. 8. Time constant with respect to spring constant of DSM .

that the variation of the wire tension can be effectively attenuated by damping the DSM. However, the modal loss factor decreases as the spring constant of the DSM increases. Although the damping coefficient is large, the deformation of the DSM is too small to exhibit any damping ability.

The time constant, defined as $T = 1/\omega_n\xi$, is used to represent the decay rate of the system after loading an impulse, and a shorter time constant achieves greater stability. The time constant is illustrated in Fig. 8. The minimal value of the time constant for the system without wire spool inertia is 0.48 s when k_m = 1500.0 N/m. When k_m is greater than 1500.0 N/m, the time constant increases very slightly. For another system, the minimal time constant is 3.7 s and occurs at k_m = 1000.0 N/m. When k_m increases, the time constant also increases. The optimal time constant for the system without wire spool inertia is at least eight times that of the original system. Therefore, the optimal time constant can be easily obtained, provided an appropriate DSM is mounted on the system.

5. Experiment

To test the performances of wire spool inertia isolation and the DSM, the wire transport system of a commercial WEDM machine (JS W-A30) is equipped with a DSM to cut an SKD11 mold steel. The machining parameters and those of the DSM are respectively shown in Tables 3 and 4. The wire passes through the tension meter and the DSM after the tension reel and then enters the upper wire guide. The wire tension is measured using a fast Fourier transform analyzer (LDS RT Photon Pro).

5.1 Step response of wire tension

In this experiment, the wire tension setting is about 1000.0 gf and the wire transport system starts from a stationary state. The wire tension recorded during the process is shown in Fig. 9. For the original system, the wire tension increases to a maximal overshoot of 1385 gf at t = 0.23 s

Table 3
Program setup of WEDM.

Machining program	Value
On time	0.8 μs
Off time	8 μs
Arc on	0.7 μs
Arc off	10 μs
Servo voltage	28 V
Wire tension	1000 gf
Wire feed	10.2 m/min
Feed rate	0.4 mm/min
Flushing pressure	0–1 kg/cm^2

Table 4
Parameters of DSM.

	Constrained layer (ABS)	Viscoelastic layer (Bitumen)
Length (m)	0.06	0.06
Width (m)	0.02	0.02
Thickness (m)	0.002	0.002
Layer number	4	3

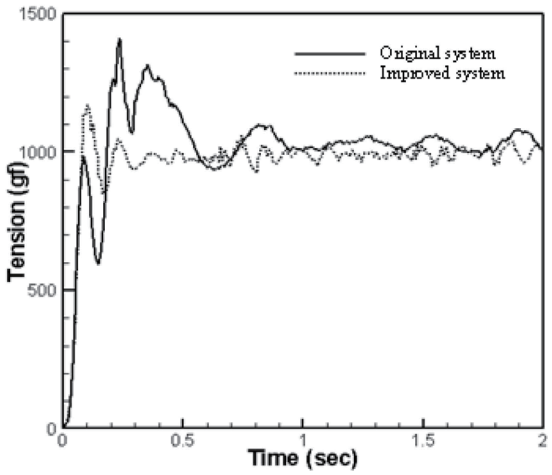

Fig. 9. Step response of the wire transport system.

and gradually decays to 1000.0 gf. When t = 0.888 s, the wire tension reaches a steady state (5% steady-state error). For the system with the DSM and wire spool inertia isolation, the maximal overshoot of the wire tension is 188.8 gf at t = 0.1 s. The oscillation frequency is significantly higher than that of the original system, indicating that the maximal overshoot, settling time, and rising time are greatly improved. When wire tension fluctuates, the variation of the tension can be eliminated more rapidly.

5.2 Steady-state response of wire tension

Figure 10 illustrates the wire tension in the time domain when the wire transport system operates in a steady state. Peaks of the original system occur at 2–3, 19, and 37 Hz, which are respectively the first and second resonant frequencies and the rotary frequency of the windup motor. The variation is 176 gf and the standard deviation is 31.5 gf.

After isolating the wire spool inertia, the main oscillation frequency increases to 9.0 Hz, the variation range is 125 gf, and the standard deviation is 15.1 gf. Hence, isolating the wire spool inertia significantly increases the fundamental frequency and the system stability. In addition,

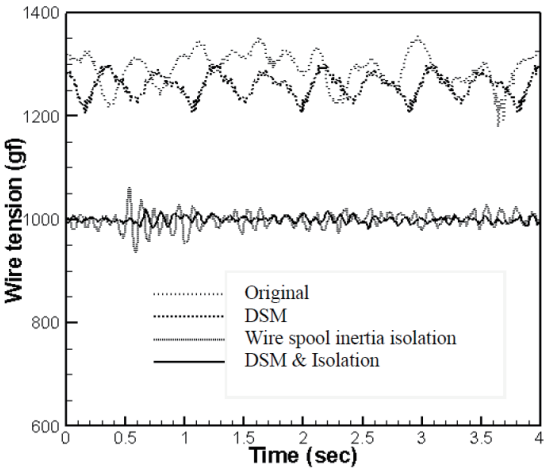

Fig. 10. Steady-state wire tension.

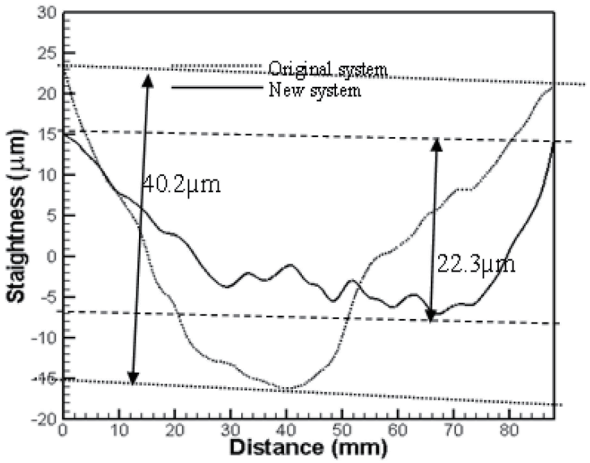

Fig. 11. Surface profile of the 10-cm-thick workpieces.

the average wire tension is reduced by 260 gf under the same input voltage for the tension reel. This is due to the rotary friction of the wire spool being canceled by the wire feed motor, thus eliminating the need for the windup motor torque to rotate the wire spool. When the system is only equipped with the DSM, the tension variation is 95 gf and its standard deviation is 21.4 gf. The fundamental frequency is almost identical to that of the original system. However, the wire tension in the frequency range of 20–50 Hz is lower than that of the original system. These results demonstrate that the DSM is more effective in the high-frequency range. If the wire spool inertia is excluded, the low main oscillation frequency renders the DSM ineffective.

When the system is equipped with both devices, the average wire tension is 260 gf lower than that of the original system. The main oscillation frequency is 9–10 Hz and the variation is 48 gf (with a standard deviation of 6 gf). This result implies that mounting both devices on the system improves its stability.

5.3 Straightness of workpiece

To identify the impact of wire tension stability on the resulting straightness, a workpiece is produced using 10-cm-thick SKD11 mold steel. The wire tensions of the original system and the new system are both tuned to 1000 gf, while the other machining conditions are kept constant. Figure 11 shows the results, where the respective straightness values for the original and new systems are 40.2 and 22.3 μm. This result verifies that the new wire transport system improves straightness by up to 44.5% under the same wire tension level. The increased wire tension stability improves the lateral vibration of the wire and thus improves the straightness.

6. Conclusions

A system dynamic approach for improving the wire tension stability in WEDM is proposed. An angle sensor is employed to keep the wire feed rate in sync with the windup rate, effectively

isolating the wire spool inertia. Then a DSM is employed to increase the damping factor of the wire transport system. The performances are theoretically investigated and experimentally validated on a commercial WEDM machine. The theoretical analysis shows that the fundamental frequency and damping factor can be effectively increased, thus increasing the stability of the wire transport system. Experimental results demonstrate that the variation of the wire tension can be reduced by 73%. When cutting a 10-cm-thick mold steel workpiece, the workpiece straightness was improved by 45%.

References

1 A. B. Puri and B. Bhattacharyya: J. Mater. Process Tech. **14** (2003) 295. https://doi.org/10.1016/S0924-0136(03)00280-2
2 A. Okada, Y. Uno, M. Nakazawa, and T. Yamauchi: CIRP Ann. Manuf. Technol. **59** (2010) 231. https://doi.org/10.1016/j.cirp.2010.03.073
3 M. Kinoshita and H. Obara: U.S. Patent No. 4622450 (1986).
4 W. L. Dekeyser and R. Snoeys: Int. Symp. ElectroMach. ISEM-**9** (1989) 226.
5 D. F. Dauw and E. Beltrami: Ann. CIRP **43** (1994) 193. https://doi.org/10.1016/S0007-8506(07)62194-5
6 G. Gamo, M. Kinoshita, and H. Obara: U.S. Patent No. 4546227 (1985).
7 G. Gamo, M. Kinoshita, and H. Obara: U.S. Patent No. 4523073 (1985).
8 M. Kamiguchi, M. Ito, and T. Ogata: U.S. Patent No. 5756954 (1988).
9 T. Magara, T. Yatomi, H. Yamada, and K. Kobayashi: J. Jpn. Soc. Elec. Mach. **25** (1991) 23. https://doi.org/10.2526/jseme.25.23
10 K. D. Murphy and Z. Lin: Int. J. Mech. Sci. **42** (2000) 1369. https://doi.org/10.1016/S0020-7403(99)00064-8
11 F. Han, G. Chenga, Z. Fenga, and S. Isagoc: Int. J. Mach. Tool. Manu. **48** (2008) 922. https://doi.org/10.1016/j.ijmachtools.2007.10. 024
12 P. W. Wang and C. S. Yang: ASME J. Micro Nano-Manuf. **1** (2013) 021006. https://doi.org/10.1115/1.4024266
13 P. W. Wang and G. B. Chen: Chin. J. Mech. Eng. **37** (2016) 325. https://doi.org/10.29979/JCSME
14 H. Morishitam, Y. Terada, M. Tomisawa, and Y. Kikuiama: U.S. Patent No. 5166490 (1992).
15 H. Obara and S. Izumiya: U.S. Patent No. 5039834 (1991).
16 H. Morishitam, Y. Terada, K. Tsurumoto, and A. Ito: U.S. Patent No. 5216217 (1993).
17 iD SERIES WIRE EDM – EX-Factory: https://www.exfactory.com (accessed April 2010).
18 M. T. Yan and P. H. Huang: Int. J. Mach. Tool. Manu. **44** (2004) 807. https://doi.org/10.1016/j.ijmachtools.2004.01.019

About the Authors

Pi-Wen Wang received his B.S., M.S., and Ph.D. degrees from Chun Cheng University, R.O.C., in 1997, 1999, and 2005, respectively. From 2005 to 2013, he was an assistant professor at Huafan University, R.O.C. Since 2013, he has been an associate professor at Huafan University. His research interests are in vibrations, acoustics, and electroacoustics. (meewpw@cc.hfu.edu.tw)

Chao-Lun Liu received his B.S. degree from National Taiwan University of Science and Technology, R.O.C., in 1976 and his M.S. degree from Huafan University, R.O.C., in 2012. From 2013 to 2022, he was a Ph.D. student at Huafan University, R.O.C. His research interests are in electroacoustics and structural dynamics. (lawrenceliu868@gmail.com)